BOSTON UNIVERSITY

COLLEGE OF ENGINEERING

Thesis

OXIDATION
OF SILICON IN CHLORINE CONTAINING AMBIENTS

BY

MITRA NAVI

B.S., FITCHBURG STATE COLLEGE, 1988

Submitted in partial fulfillment of the
requirements for the degree of
Master of Science in Electrical Engineering
1993

Abstract

One of the techniques routinely used to form thin and highly reliable oxides is the addition of chlorine species to the oxidizing ambient during gate oxide formation. The benefits that have been reported include passivation of alkali ions, higher and more uniform oxide dielectric strength, and improved junction properties due to lower leakage. In this work, the film growth kinetics, chlorine incorporation and oxidation enhanced diffusion of phosphorus during oxide growth in TCA/O_2 ambients are investigated. In order to study Cl-incorporation and oxidation kinetics, $\langle 100 \rangle$ silicon wafers were oxidized in dry O_2 and TCA/O_2 with 1-4% equivalent HCl percentage. SIMS measurements were used to characterize the effect of chlorine incorporation in the film show strong incorporation near the Si/SiO_2 interface. This incorporation increases for longer oxidation times, but is nearly independent of TCA percentage. Parabolic and linear rate constants were extracted form the oxide thickness as a function of time and a nonlinear dependence on partial pressure of TCA was observed, with the greatest change for small percentages of TCA. Oxidation enhanced diffusion (OED) of phosphorus has also been characterized in TCA/O_2 ambients. Spreading resistance measurements show a reduction in supersaturation of interstitials relative to oxidation in dry O_2. Like the oxide growth kinetics, the reduction has a nonlinear dependence on partial pressure of TCA.

Contents

List of Tables

List of Figures

Chapter 1

Introduction

The advancement of VLSI technology requires increasing number of devices on a single chip. One of the ways to achieve this goal is to shrink the dimensions of the device structure. In MOS technology, the miniaturization procedure calls for scaling down of all physical dimensions, among which a very important one is the gate oxide thickness. To realize a sub-micron MOS channel, the dimension of the gate oxide must be scaled down to the order of 100Å or less. One of the techniques routinely used to form thin and highly reliable oxides is addition of chlorine species to the oxidizing ambient during gate oxide formation. The benefits that have been reported include passivation of mobile ions [1], enhancement of minority-carrier lifetime in silicon [2], improvement of the oxide dielectric breakdown strength [3] and improved threshold stabilities. However, if the process is done inappropriately, the use of chlorine can lead to catastrophic results, including separation of the oxide from the underlying silicon and etching of the silicon surface [2].

In recent years, there has been much interest in the study of chlorine and hydrogen incorporation during oxide growth. Inspection of SIMS profiles show that a significant amount of Cl is distributed in the oxide, with increasing concentration towards the SiO_2/Si interface [2]. This incorporation changes the structure of the oxide and affects oxidation kinetics and point defect interactions in the silicon bulk.

When Cl-species are used during the oxidation of Si, an enhanced oxidation rate is observed. This increase is reflected in both parabolic and linear rate constants. It has been suggested that incorporated Cl provides an alternative path for oxidation. It has also been reported that the Cl species (HCl, TCA, TCE, etc) decompose in the gas phase where the reaction products are known to affect the oxide growth rate.

It is known that the presence of chlorine in an oxidizing ambient causes a reduction in oxidation enhanced diffusion (OED) of impurities in silicon. This effect can be related to vacancy generation or reduction of supersaturation of interstitials at the interface. Either way, Cl-incorporation at Si/SiO_2 region seems to alter the interface reactions.

The objective of this work is to investigate the relationship between Cl-incorporation, oxidation kinetics and OED/ORD effects seen in oxides grown in Cl-ambients in order to better understand oxidation in chlorine-containing ambients. Chapter 2 gives a brief explanation of Deal and Grove's linear-parabolic model for thermal oxidation of silicon. We also review current models for oxidation kinetics in Cl-containing ambients and how Cl-incorporation alters the oxidation rate. OED/ORD effects are presented next, as point defect interaction and diffusion of dopants in the bulk of Si in presence of Cl species in the oxide is discussed. Chapter 3 describes the experiments conducted for this work. Our experimental work is divided in to three major thrusts: Oxidation kinetics experiments which include a series of thickness measurements for oxides grown at different TCA (trichloroethane, a Cl source) partial pressures for different times and temperatures; SIMS measurements of incorporated Cl for different times and TCA partial pressures; and OED/ORD experiments done by studying the enhanced diffusivity of a phosphorus marker layer using spreading resistance. In Chapter 4 we discuss our experimental results and present a qualitative model for chlorine incorporation. The oxidation kinetics and OED/ORD results are also discussed in this chapter. Chapter 5 summaries the result of this work and additional work is suggested at the end of Chapter 5.

Chapter 2

Background

Experimental observations have indicated that the addition of a chlorine species to the oxidizing ambient affects the oxidation kinetics and dopant diffusion in the bulk of silicon. During thermal oxidation of silicon, a large amount of Cl is incorporated at the interface of Si/SiO_2. As a result, the diffusion and reaction fluxes of oxidizing species in the oxide are altered.

In this chapter, we discuss the effect of chlorine species on oxidation kinetics and dopant diffusion. First we examine the oxidation process and look at how Cl-incorporation affects the oxidation kinetics. A review of existing models, describing the effect of Cl on oxidation kinetics is presented next. Finally we discuss dopant diffusion in the bulk of Si and examine how point-defect interactions are altered in the presence of Cl-species.

2.1 Oxidation Kinetics

Deal and Grove [5] were among the first to develop a linear-parabolic model for oxidation of silicon in both dry O_2 and steam ambients. They assumed that oxidation proceeds by the inward movement of a species of oxidant. The transported species must go through the following stages:

- It is transported from the bulk of the gas to the gas-SiO_2 interface where it reacts or is adsorbed.
- It is transported across the oxide film towards the Si-SiO_2 interface.
- It reacts with Si at the Si-SiO_2 interface to form SiO_2.

The assumption is made that oxidizing species diffuse rapidly across the oxide, so the oxidation process is in steady state and the flux of oxidants from each of the above steps are equal. The flux of oxidants from gas to outer surface of oxide is taken to be

$$F_1 = h\,(C^* - C_{\mathrm{o}}), \tag{2.1}$$

where h is a gas–phase transport coefficient, C_{o} is the concentration of oxidant at the outer surface of oxide at any given time and C^* is the equilibrium concentration of oxidant in the oxide. The equilibrium concentration of oxidant is related to partial pressure of the oxidant by

$$C^* = Kp, \tag{2.2}$$

where K is Henry's constant for the oxidant species.

The flux of oxidant across the oxide is assumed to be given by Fick's law,

$$F_2 = -D_{\mathrm{eff}}\left(\frac{dC}{dx}\right), \tag{2.3}$$

where D_{eff} is the effective diffusion coefficient and dC/dx is the concentration gradient of oxidizing species across the oxide.

Finally, the flux of oxidizing species due to reaction at the interface is given by

$$F_3 = k_i C_i. \tag{2.4}$$

where C_i is the interface concentration of oxidizing species and k_i is the oxidation reaction rate constant. Setting these fluxes equal and solving for oxidation rate we have,

$$\frac{\partial x_{\mathrm{o}}}{\partial t} = \frac{F}{N_1} = \frac{k_i C^*}{N_1\,(1 + k_i/h + k_i x_{\mathrm{o}}/D_{\mathrm{eff}})}, \tag{2.5}$$

where N_1 is the number of oxidant molecules in a unit volume of oxide layer. Using the initial condition of $x_{\mathrm{o}} = x_{\mathrm{i}}$ at t=0, and integrating above equation we have,

$$\frac{{x_{\mathrm{o}}}^2 - x_i^2}{A} + \frac{x_{\mathrm{o}} - x_i}{B/A} = t, \tag{2.6}$$

or

$$ {x_{\mathrm{o}}}^2 + Ax_{\mathrm{o}} = Bt + x_i^2 + Ax_i, \tag{2.7}$$

which can be rewritten in the form

$$ {x_{\mathrm{o}}}^2 + Ax_{\mathrm{o}} = B(t + \tau), \tag{2.8}$$

where

$$A = 2D_{\mathrm{eff}}\left(1/k_i + 1/h\right), \tag{2.9}$$

$$B = 2D_{\mathrm{eff}}C^*/N_1, \tag{2.10}$$

and

$$\tau = x_i\left(x_{\mathrm{i}} + A/B\right), \tag{2.11}$$

Solving the quadratic Equation of 2.8

$$x_{\mathrm{o}} = \frac{A}{2}\left[\left(1 + \frac{t+\tau}{A^2/4B}\right)^{1/2} - 1\right], \tag{2.12}$$

which gives the oxide thickness as a function of time. At relatively large times (t $>> A^2/4B$)

$$ {x_{\mathrm{o}}}^2 \cong Bt, \tag{2.13}$$

which is the well known parabolic oxidation law for relatively long times.

2.1.1 Effect of Chlorine Species on Oxidation Kinetics

For a given silicon orientation and temperature, the rate of oxidation is increased when Cl-species are present in the oxidizing ambient. The most widely used sources of Cl are HCl, TCA, TCE and Cl_2 [6]. Due to safety concerns and special installation

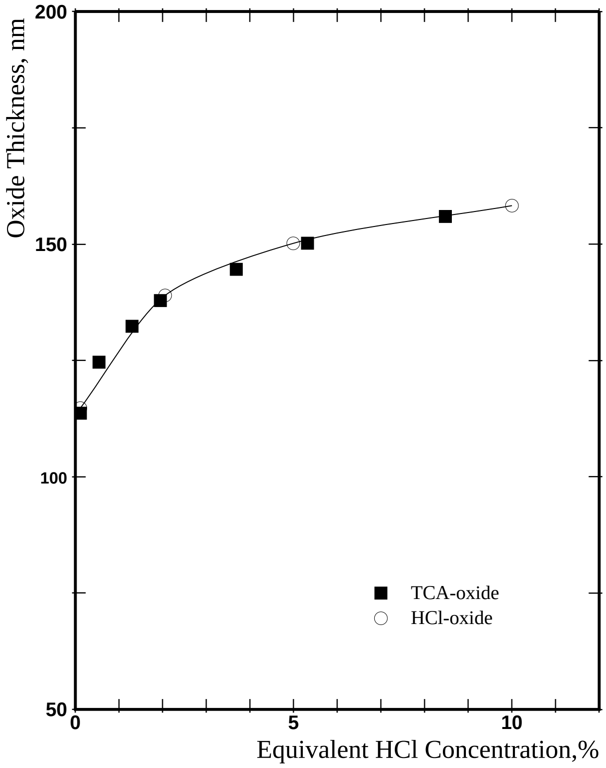

Figure 2.1: The increase in oxide thickness by the use of HCl and TCA is given as a function of effective HCl concentration. Data from Kriegler and Janssens [7].

requirements involved with the use of Cl_2 and HCl, other sources such as TCE and, most commonly TCA are being used extensively. It has been shown [8] that there is a direct correlation between the effects of TCA and HCl on oxidation of silicon. TCA (1,1,1-trichloroethane) is similar to HCl in having a chlorine to hydrogen ratio of unity, where 1% TCA is roughly equivalent to 3% HCl. When TCA is used in the gas phase we have the following gas phase, reactions, the first of which goes to completion:

$$C_2H_3Cl_3 + 2O_2 \rightarrow 3HCl + 4CO_2 \tag{2.14}$$

$$4HCl + O_2 \leftrightarrow 2H_2O + 2Cl_2 \tag{2.15}$$

Figure 2.2: Parabolic and linear rate constants versus volume percent of H_2O in O_2. Data from Deal[9] *et al.*

The similarity of HCl and TCA sources on oxide growth have been investigated by number of researchers [7, 8]. Figure 2.1 illustrates that an identical oxide thickness is grown for both TCA and and its corresponding equivalent HCl. In our experimental procedure, the source of chlorine used is TCA. Since the two sources, HCl and TCA, are equivalent, to be consistent with previous work, we will use the equivalent HCl percentage instead of TCA percentage (which is just a factor of three smaller).

It can be seen from reaction 2.15 that water and chlorine are present in addition to O_2 and HCl. It is known that small additions of H_2O to the oxidizing ambient can increase the oxidation rate significantly [10]. Therefore the existence of steam in the ambient could well contribute to changes in the oxidation process. If this is the case and the reaction of HCl and O_2 goes nearly to completion then 2 moles of HCl will produce 1 mole each of H_2O and Cl_2. The O_2/HCl data can therefore be compared with the results obtained from equivalent O_2/H_2O oxidation. Inspecting Deal and Plummer's data in Figure 2.3 and 2.4 for the case of 10% HCl in O_2 and 5% H_2O in O_2 at 900, 1000 and 1100°C, it can be noted that the 5% H_2O rates are significantly greater than for 10% HCl, especially at 900°C (about 30%). Since the addition of Cl_2 alone to a dry O_2 ambient increases the oxidation rate, these observations lead to the conclusion that the O_2-HCl gas phase reaction 2.15 does not go to completion. Thermodynamic gas phase calculations of Van der Meulen *et al.* predict that only about 30% of the HCl oxidizes to give steam. When these calculations were used to estimate the steam concentration in the gas, including the effect of steam alone substantially underestimates the increase in oxidation rate. Furthermore, when parabolic and linear rates were plotted versus HCl concentration [9], a nonlinear increase in B and B/A was observed going from 0 to 1% HCl. This general trend has also been reported for oxidation in O_2/H_2O, where the nonlinear effect is much less pronounced (see Figure 2.2). This nonlinearity can be related to structural changes in the oxide. Incorporation of chlorine and hydrogen can relax the structure of the oxide and result in enhancement of oxidant diffusivity. This idea will be discussed in more detail later on in this chapter.

Hirbayashy and Iwamura derived a general relationship including the combination of species present. They assumed that the flux of the two oxidizing species (e.g., H_2O and O_2) are parallel but independent. In deriving their model they considered the fluxes of oxidizing species across the oxide and assumed that the reaction rates of the oxidizing species at the interface are increased due to presence of HCl. The following is the final form of their model:

$$t = \frac{1}{E}\{({x_o}^2 - x_i^2) + C(x_o - x_i) - D\ln\left[\frac{2Ex_o + F}{2Ex_i + F}\right]\} \tag{2.16}$$

where

$$C = \frac{A_1B_1 + A_2B_2}{B_1 + B_2}, \tag{2.17}$$

$$D = \frac{B_1B_2(A_1 - {A_2}^2)}{2{(B_1 + B_2)}^2}, \tag{2.18}$$

$$E = B_1 + B_2, \tag{2.19}$$

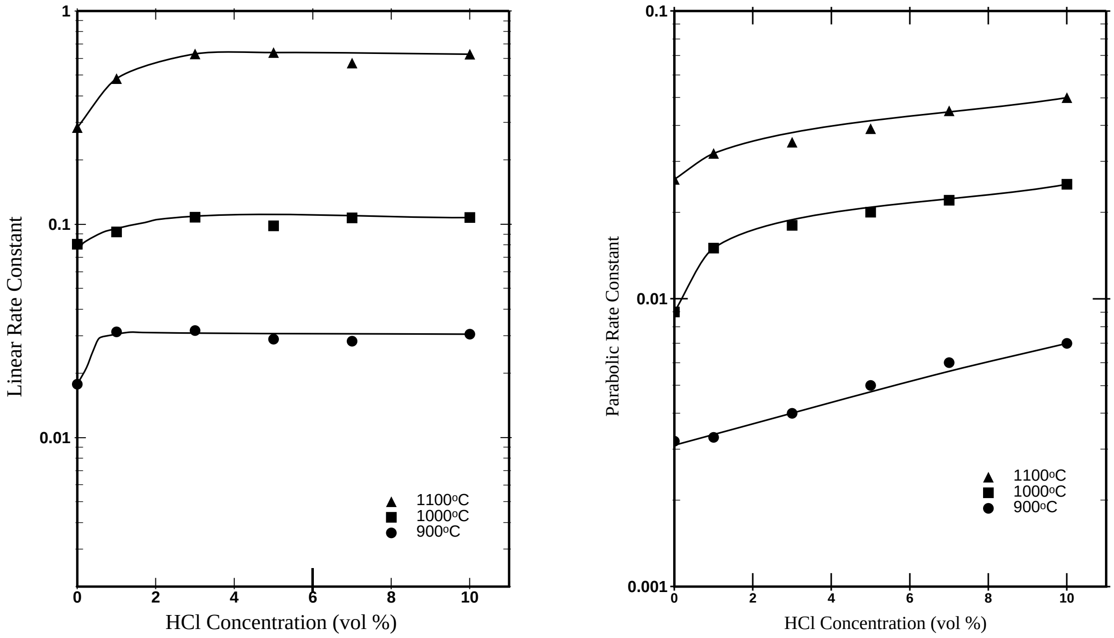

Figure 2.3: Parabolic and linear rate constants versus % HCl concentration. Data from Deal [9] *et al.*

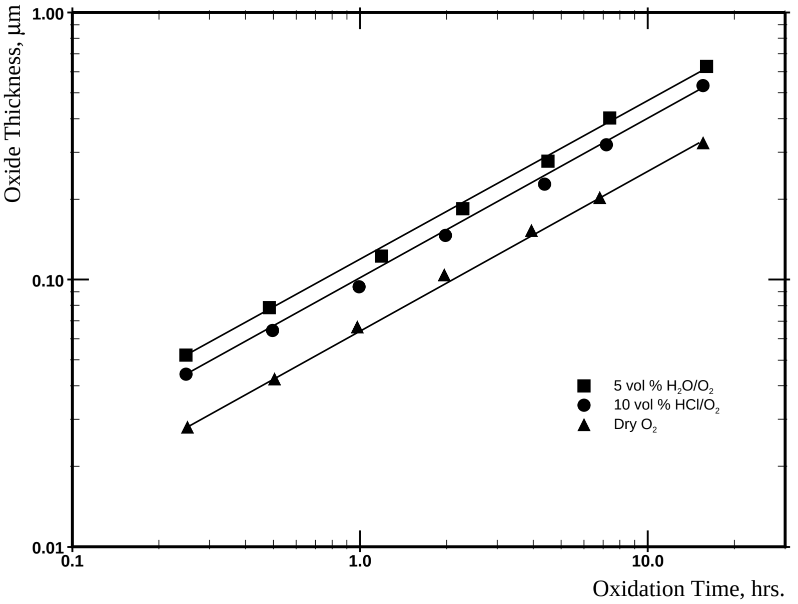

Figure 2.4: Oxide thickness vs. oxidation time for 5 vol% H_2O/O_2, 10 vol% HCl/O_2, and dry O_2 for 1000°C ⟨111⟩ data from Deal [9] *et al.*

$$F = A_1B_2 + A_2B_1. \tag{2.20}$$

A_1 and B_1 are the oxidation parameters for the first species and A_2 and B_2 are the parameters for second species. They fitted oxide thickness as a function of time to Equation 2.16 and calculated the effective B and B/A. They reported negative values of A for $\langle 110 \rangle$ and $\langle 311 \rangle$ orientations, which suggests the growth rate does not follow the linear-parabolic relationship, especially beyond 3% HCl. Considering the definition of the parabolic (B) and linear (B/A) rate constants from Equations 2.9 and 2.10 suggests that the increase in B with HCl concentration is most likely related to the effective diffusivity coefficient D_{eff}. Likewise it appears that the similar increase in both B and B/A might be related to solubility of oxidizing species. In light of above argument, the increase of the parabolic rate constants with increasing HCl concentration is likely to be related to the incorporation of chlorine, since it has been established that a higher concentration of chlorine is incorporated into SiO_2 film as the HCl concentration and/or the silicon oxidation temperature are increased [12]. Consequently, it might be anticipated that increasing the chlorine concentration would cause the SiO_2 lattice to be less strained (especially near the interface), thus allowing diffusion of oxidant to occur more easily, and thereby increase the oxidation rate as observed in the oxidation of heavily boron-doped silicon [13].

2.2 Incorporated Chlorine in the Oxide

The chlorine distribution in oxides grown in a chlorine containing gas ambient has a strong influence on the physical properties of the Si-SiO_2 system. The incorporation of chlorine atoms in the SiO_2 layer has been studied by means of large variety of analytical techniques such as nuclear backscattering, secondary ion mass spectrometry (SIMS), Auger spectroscopy, electron microprobe and Rutherford backscattering of alpha particles. All the different experimental techniques confirm that most of the

Figure 2.5: Concentration profiles for incorporated Cl and gas species in the oxide

chlorine piles-up in the oxide near the interface. It has been shown that the chlorine peak height increases with oxidation temperature, and increasing oxidation time or oxide thickness results in increasing peak heights at a given HCl percentage or oxidation temperature.

The process of Cl-incorporation has been described by Sheu *et al.* as follows. In the course of oxidizing silicon, molecular oxidant species (O_2 and, if appropriate, H_2O) and molecular Cl species (Cl_2 and, if appropriate, HCl) are dissolved at the oxide-gas interface. These species diffuse to the SiO_2-Si interface, where they react with the Si and form an incremental silicon dioxide network incorporating bonded H and Cl impurity species ($\equiv$Si $-$ Cl, $\equiv$Si $-$ OH, $\equiv$Si $-$ H). Figure 2.5 is a schematic presentation of various concentration profiles involved in the model. The chlorine concentration versus depth profile, determined by bonded species in the oxide network, is very nonuniform, increasing monotonically with depth in the oxide film (see any single SIMS profile in Figure 2.6). In order for this to occur, there must be some "replacement reaction" such as

$$\equiv \mathrm{Si} - \mathrm{Cl} + \mathrm{H_2O} \rightarrow \equiv \mathrm{Si} - \mathrm{OH} + \mathrm{HCl} \tag{2.21}$$

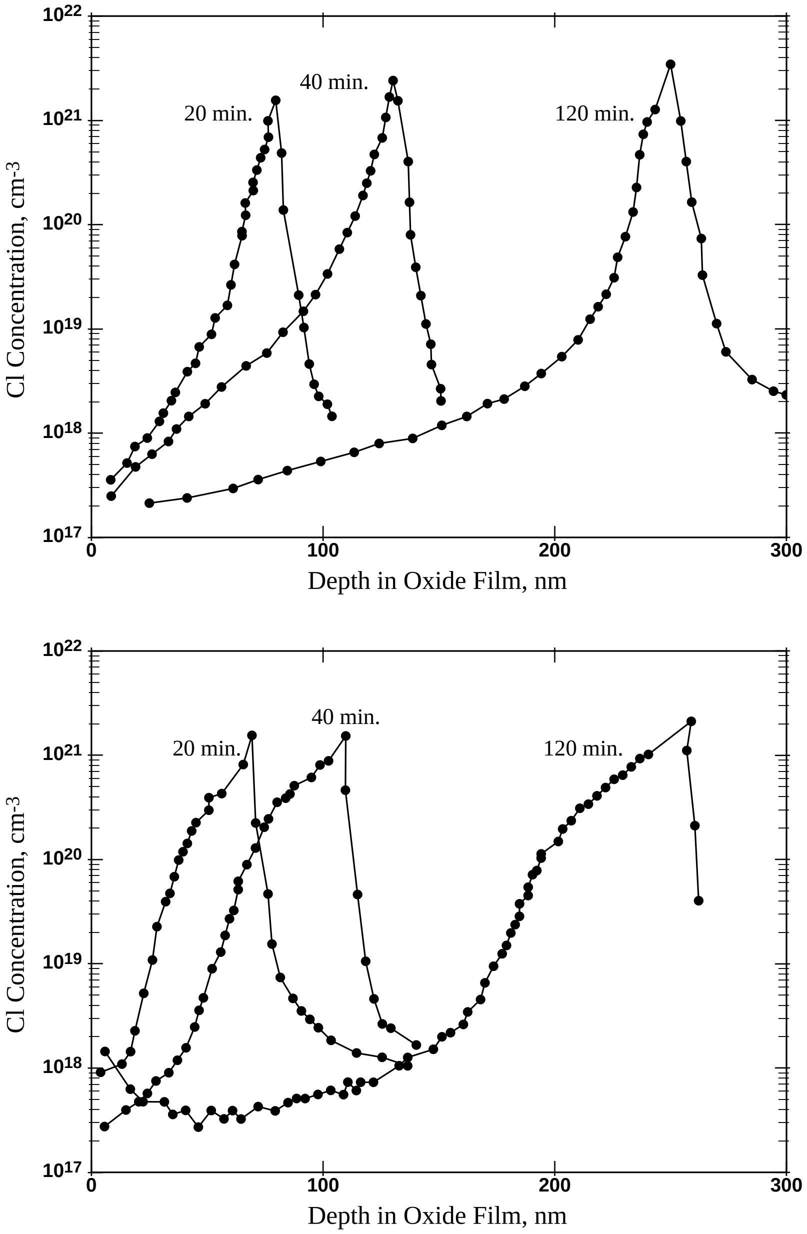

Figure 2.6: Chlorine concentration profiles from Sheu [13] *et al.* for oxidation at 1100°C for 20, 40, 120 min (a) in 2% HCl/O_2 ambients and (b) in 0.3% Cl_2/O_2 ambients.

which releases the bonded Cl from the oxide network. This reaction decreases the bonded Cl concentration and increases the molecular Cl concentration at a given distance from the oxidizing interface. The shape of the near-interface Cl profile in a Cl_2 oxide is very different from that in an HCl oxide. The rate at which the Cl concentration changes with distance from the interface is directly related to the kinetics of the bonded Cl "replacement" reaction. In Cl_2 oxide, molecular oxygen (O_2) is the predominant species available to replace bonded Cl. The difference in profile shape for the two types of oxide therefore implies that O_2 replaces bonded Cl at a much slower rate than does H_2O. Deal reported that no real chlorine incorporation is noticed for oxide grown in HCl/H_2O ambients. This observation is in agreement with the results of Van der Meulen *et al.* [16], which indicates that any Cl build up in the oxide layer rapidly disappears by a subsequent wet oxidation step.

For higher temperatures and HCl partial pressures, existence of microstructures have been reported by several workers [12, 15]. It has been shown that if the oxidation is carried out for too long a time with too much chlorine, the oxide can bubble up from the silicon. Under extreme conditions the oxide separates completely from the silicon. The bubbling up of the oxide is believed to be a result of a build-up of a gas at the interface. Mass spectrometric analyses have shown this gas to be some form of silicon chloride [12]; this is further substantiated by the etching of the silicon surface that occurs concurrently with the separation of the oxide.

2.3 Point Defect Interactions during Oxidation

It is generally accepted that thermal oxidation of silicon results in the generation of excess silicon point defects in Si-SiO_2 interface during oxidation. The process can be described as follows. During oxidation in dry O_2, the oxidant species diffuse through the oxide. They react at the interface, which results in the insertion of oxygen atoms between silicon lattice. This reaction requires a volume expansion, thus oxidation tends to build up strain in the lattice at the interface. Therefore, some mechanism is required to provide the free volume necessary to allow the reaction to continue.

There are three main mechanism by which the free volume constraint at the interface is satisfied: viscoelastic flow of the oxide near the interface [29], absorption of silicon vacancies that diffuse from the Si [17] and creation of silicon interstitials at the interface and their diffusion into the silicon and the oxide. Viscoelastic flow occurs when compressive stresses near the interface causes the newly formed oxide to flow away from the interface.

The other two mechanisms involve the interaction with silicon point defects. As the oxidation reaction proceeds, the number of vacancies in the bulk are depleted which results in an undersaturation of vacancies. The alternative is the creation of silicon interstitials at the interface. These interstitials generated can diffuse into the bulk of silicon or into the oxide. Interstitials injected in the oxide can react with the oxidizing species [18]. On the other hand, interstitials injected into the bulk increase the density of point defects and result in oxidation enhanced diffusion of dopant impurities, since diffusion of substitutional impurities in the crystal requires the interaction of point defects.

The diffusivity of dopants in silicon is related to the concentration of point defects via:

$$\frac{D_{\mathrm{imp}}}{D^*_{\mathrm{imp}}} = f_{\mathrm{I}}^{\mathrm{imp}} \frac{C_{\mathrm{I}}}{C^*_{\mathrm{I}}} + \left(1 - f_{\mathrm{I}}^{\mathrm{imp}}\right) \frac{C_{\mathrm{V}}}{C^*_{\mathrm{V}}}, \tag{2.22}$$

where C^*_{I} and C^*_{V} are the equilibrium concentration of silicon interstitials and vacancies respectively, and $f_{\mathrm{I}}^{\mathrm{imp}}$ represents the fraction of the equilibrium impurity diffusion coefficient (D^*_{imp}) that is due to the interstitial mechanisms. The value of $f_{\mathrm{I}}^{\mathrm{imp}}$ will vary according to the substitutional impurity involved, as well as the diffusion temperature.

Thermal oxidation of silicon is also known to cause the growth of stacking faults in the bulk of silicon. Stacking faults are interstitial-type defects which consist of extra partial planes of silicon atoms lying along ⟨111⟩ planes, and their growth depends on the concentration of point defects [18]. Since oxidation causes a supersaturation of interstitials and undersaturation of vacancies, either of these phenomena can result in the growth of stacking faults during thermal oxidation.

2.3.1 Effect of Chlorine on Point Defect Generation

Addition of Cl species to the oxidizing atmosphere is known to alter the point defect concentration in silicon during the thermal oxidation [19, 20] . Its been suggested by a number of workers [21, 22] that addition of HCl to the oxidizing ambient can cause vacancy generation. Murarka proposed a two step mechanism where chlorine reacts with silicon atoms on the lattice sites to form some SiCl compound. During this process a silicon vacancy is generated. This vacancy is then available to recombine with a silicon interstitial produced due to oxidation.

Oh *et al.* argued that the postulate of vacancy generation at the Si/SiO_2 interface during thermal oxidation runs counter to the knowledge that SiO_2 formation generates large compressive stresses which can be reduced by the consumption of vacancies and/or generation of interstitials [23]. They suggested that it is more likely for HCl addition to alter the Si interstitial partition coefficient. They studied the diffusion of phosphorus marker layer at 1145°C in dry O_2 with various partial pressures of HCl and the junction depth differences they observed versus oxidation time for different partial pressure of HCl are shown in Figure 2.7. From these results, they postulated that HCl addition to the oxidizing ambient does not cause vacancy generation to occur at the Si/SiO_2 interface, but merely reduces the flux of Si interstitials flowing into the silicon as a consequence of the oxidation process.

As was presented in the previous section, HCl oxide is known to be structurally different from the standard oxide in that an Si-Cl complex is formed with Cl substituting for an oxygen leading to a nonbridging bond. The Cl atom plays the role of a network terminator, so that the SiO_2 network becomes less rigid in the presence

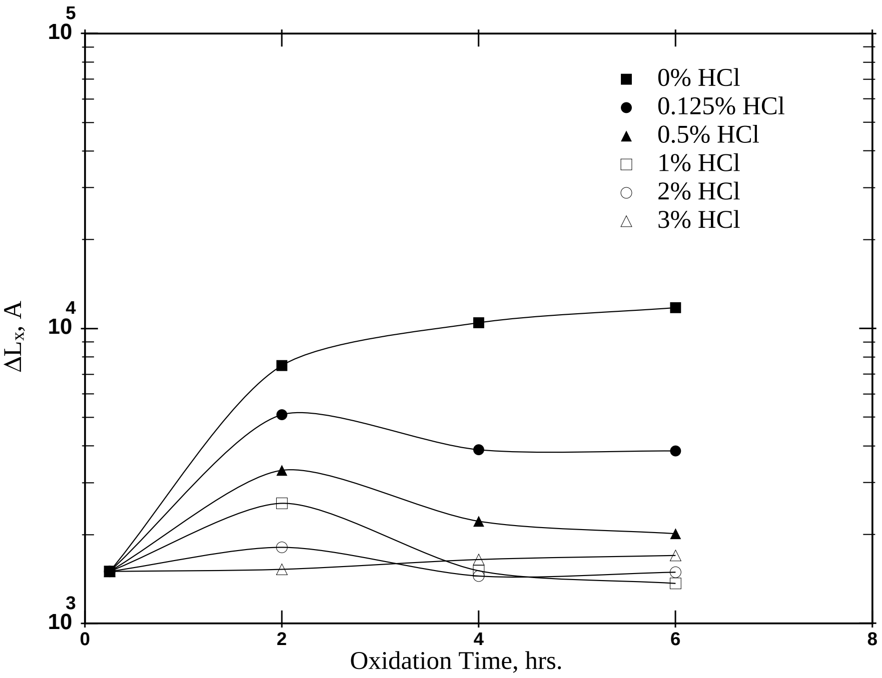

Figure 2.7: Junction depth difference under the oxide stripes compared to nitride stripes from Oh [23] *et al.*, is plotted as a function of oxidation time at 1145°C for different % HCl

of Cl. Thus, Cl-incorporation tends to reduce the built-up stress in the lattice at the interface, allowing viscous flow of the oxide. Since viscous flow helps the free volume requirement at the interface, fewer Si interstitials are generated and fewer self-interstitials are available to flow into the silicon. This reduction of network rigidity is especially important in the interface region where Cl-incorporation is at its maximum.

The experimental results of oxidation induced stacking fault growth during HCl oxidation indicates that the addition of HCl in the oxidation atmosphere suppresses the growth of OSF. The degree of suppression increases for increasing the partial pressure of HCl. This has been explained by considering a reaction of chlorine with the silicon interstitials at the interface, which reduces the supersaturation of silicon interstitials in the bulk during silicon oxidation. The reaction at the interface can be described as a sink for interstitials [22]. This phenomena is in complete agreement with the reduction of OED for dopants that diffuse via an interstitials mechanism. What is apparent from these observations is that introducing chlorine species in the ambient and their incorporation at the interface effects the concentration of point defects generated at the interface and result in reduction in OED and suppression of OISF.

Chapter 3

Experimental Procedures and Analysis Techniques

The role of chlorine during oxidation of silicon has been investigated by many workers. Oxidation kinetics, Cl-incorporation and OED/ORD effects have been characterize for a wide range of oxidation conditions. The goal of the present experiments is to obtain a consistent set of data that includes oxidation kinetics, Cl-incorporation and OED/ORD measurements to be used in understanding how these processes are related and developing models to account for the interactions. The design of experiments and the techniques used to analyze the results will be presented in this section.

3.1 Wafer Processing

The starting material for the experiments was n-type 4-inch float-zone $\langle 100 \rangle$ silicon wafers with resistivity of 500-1000 Ω–cm. N-type background doping was chosen since phosphorus was to be implanted and the presence of a junction reduces the accuracy of the spreading resistance measurements. Float-zone wafers were used to avoid interstitial generation during oxygen precipitation in Czochralski silicon. Figure 3.1 illustrates the experimental flow. The wafers were first oxidized in dry O_2 at 1000°C

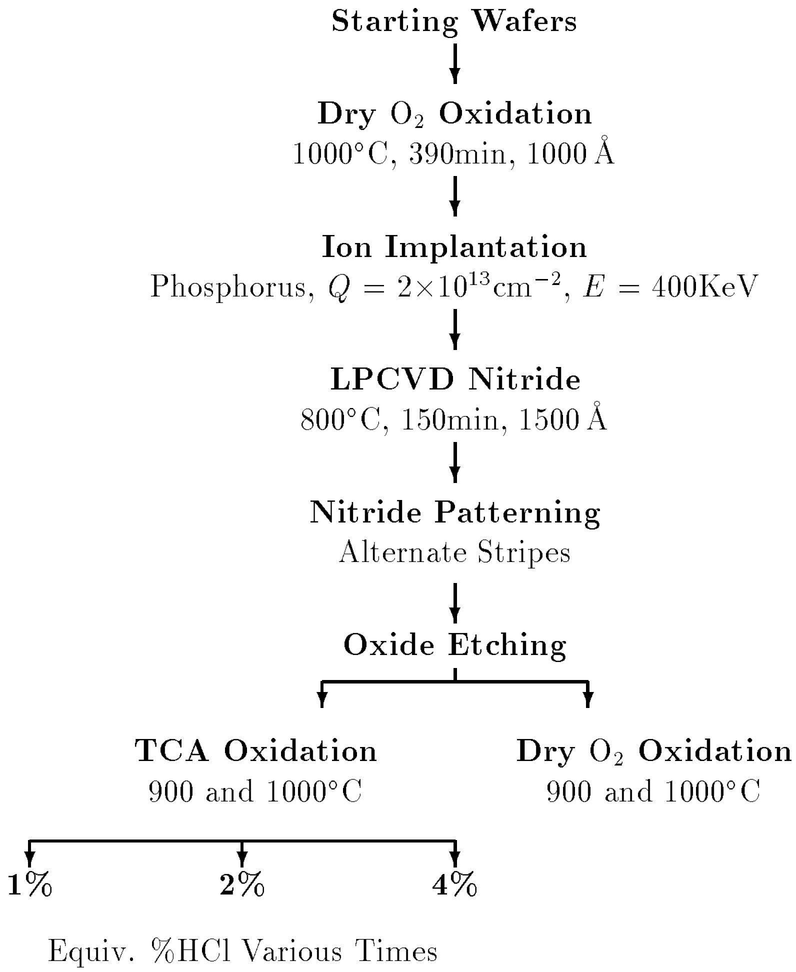

Figure 3.1: Wafer processing steps

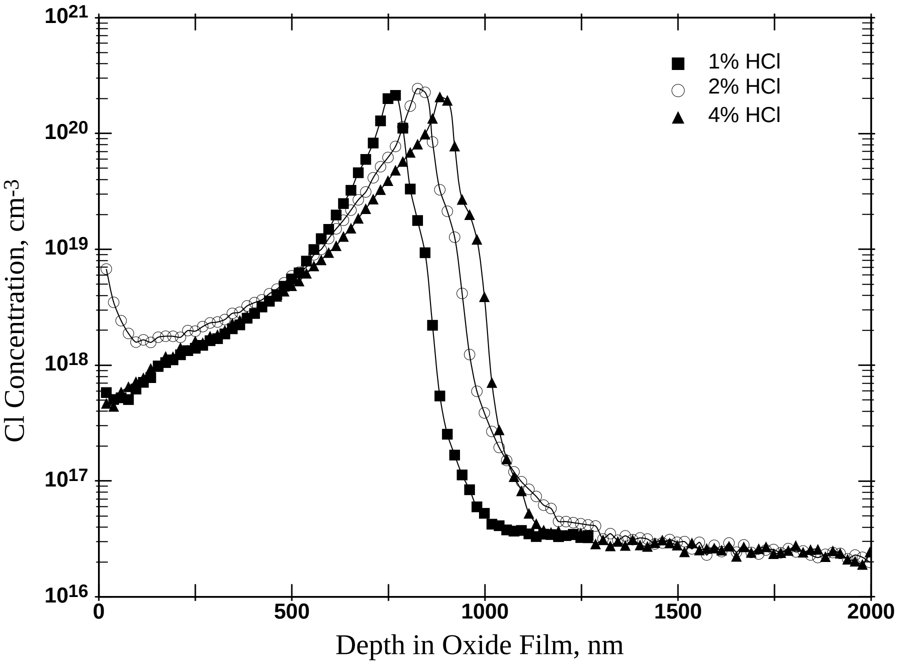

Figure 3.2: SIMS measurement of incorporated chlorine in oxides grown in 1, 2 and 4% equivalent HCl at 1000°C.

for 390 minutes to grow a pad oxide of 1000 Å. Wafers were then implanted with a dose of $2\times10^{13}\mathrm{cm}^{-2}$ at 400keV and annealed at 900°C for 30 minutes.

Next, a nitride layer of 1500 Å was deposited by low pressure CVD. The nitride layer covering the thin oxide was used as a diffusion barrier to oxidant species so that diffusion under oxidizing and non-oxidizing conditions could be carried out simultaneously. The wafers were patterned with a stripe mask to produce alternating 3mm wide stripes of bare silicon and the oxide-nitride combination. The nitride was removed using a plasma etcher and finally the wafers were immersed in buffered-oxide-etch (BOE) to remove the pad oxide, resulting in the test structure illustrated in Figure 3.3. The wafers were divided into two different sets. One set of wafers were oxidized in dry O_2 at 900 and 1000°C for 16 and 8 h, respectively. The other set were oxidized in TCA/O_2 ambients for different partial pressures of TCA.

TCA is a liquid source and is used with N_2 as a carrier gas. Equivalent HCl partial

Figure 3.3: The experimental test structure. The structure has an inert region underneath the nitride stripes and an enhanced diffusion region underneath the bare silicon in the oxidizing ambient.

pressures were calculated using the conversion graphs of J.C. Schumacher [24]. The bubbler temperature was 25°C. Oxidation was done at 900 and 1000°C for 16 and 8 h respectively for 1-4% equivalent HCl partial pressure.

To investigate the effect of chlorine on oxidation kinetics, additional experiments were done on ⟨100⟩ Czochralski-grown silicon wafers. The wafers were n-type phosphorus doped with resistivity of 10-20 Ω–cm. These wafers were oxidized in dry O_2 and TCA/O_2 with 1-4% equivalent HCl percentage as described above. Oxidations were done at 900 and 1000°C for various times and oxide thickness were measured using Nanospec and ellipsometry.

To understand the relation between the oxide growth rate and the incorporated Cl in the oxide, the Cl profile was measured by SIMS (Secondary Ion Mass Spectroscopy) performed by Evans East. The primary bombarding species were Cs^+ with ion energy of 5kev. Figure 3.2 shows examples of incorporated Cl profile for different partial pressures of TCA at 1000°C.

3.2 Measurement Techniques

The diffusion profile measurements in this work were done using spreading resistance. Two Os-W probes of spreading resistance device were polished by 0.1μm diamond paste on frosted sapphire pads until the resistance measured on the qualification samples falls in the acceptable range. The polished probes were then tested for accuracy by measuring the resistance of 8 uniformly doped calibration samples whose resistivities are known.

Wafers were scribed and cleaved into 3mm x 3mm samples. Each sample contained an enhanced and an inert diffusion stripe, to minimize the experimental errors. The samples were then beveled on 17-minute blocks in the direction perpendicular to the surface of the stripes. Angles were measured using the small angle measurement (SAM). The beveled samples were placed underneath the probes and the probes stepped down the bevel surface. 5 micron step size were used for all the measurements. Multiple measurements were done in each region to insure the accuracy of the profiles. The location of the Si-SiO$_2$ interface was determined as the point where resistance measurement dropped from some high initial value, since the oxide layer has a very large resistance. The position of the interface is very important and can affect the calculation of dopant

diffusivity. The spreading resistance profiles were converted to concentration profiles using SERAPES[1]. Profiles from samples which saw only the anneal and ramp up/down were fed into the SUPREM IV [25] program to provide an initial profiles for processing simulations. Simulation of diffusion under oxidizing and nonoxidizing conditions were performed with constant diffusion coefficients. The resulting profiles were converted back to spreading resistance data using SERAPES and compared to the data taken on the diffused wafer sections. An optimization program PROFILE [26] was used in order to get the best fit to experimental data. Figure 3.4 shows the block

---

[1] SprEading Resistance Analysis with Poisson Equation Solution

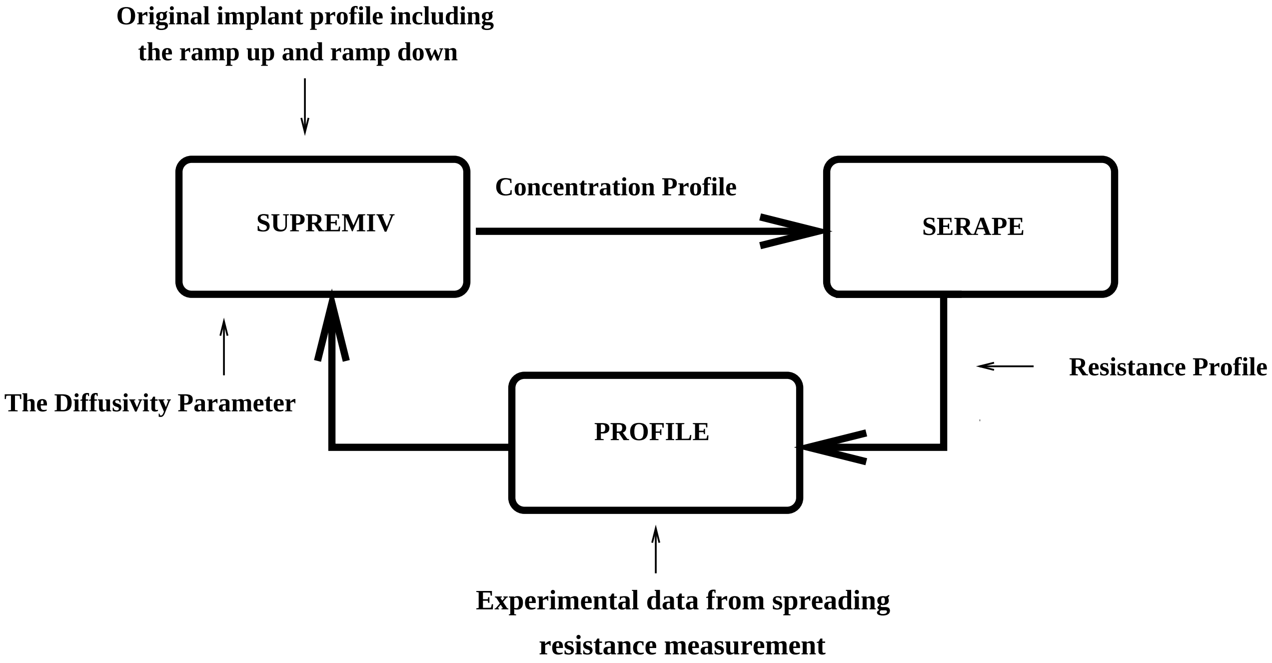

Figure 3.4: Block diagram for extracting the diffusivity parameters

diagram for extracting the diffusivity parameters.

Based on these comparisons, the value of diffusion coefficient that gave the best agreement between the simulated and measured profiles in the spreading resistance region was found. This technique was used to find the diffusion coefficient for both the oxidizing and nonoxidizing regions. Figure 3.5 shows an example of fitting the calculated profile to the measured profile.

Assuming a value of one for $f_{\mathrm{I}}^{\mathrm{imp}}$ [27] in Eq. 2.22 the interstitial enhancement ratio can be related to enhanced diffusivity via:

$$\frac{D_{\mathrm{P}}}{D_{\mathrm{P}}^{*}} \cong \frac{C_{\mathrm{I}}}{C_{\mathrm{I}}^{*}}, \tag{3.1}$$

where D_{P} is the diffusivity in the oxidizing region and D_{P}^{*} is the diffusivity under the nonoxidizing regions.

As was described previously, a series of oxide thickness measurements were done using Nanospec and ellipsometry to characterize the effect of Cl-species in the ambient on oxidation kinetics. In ellipsometric methods of oxide measurement a monochro-

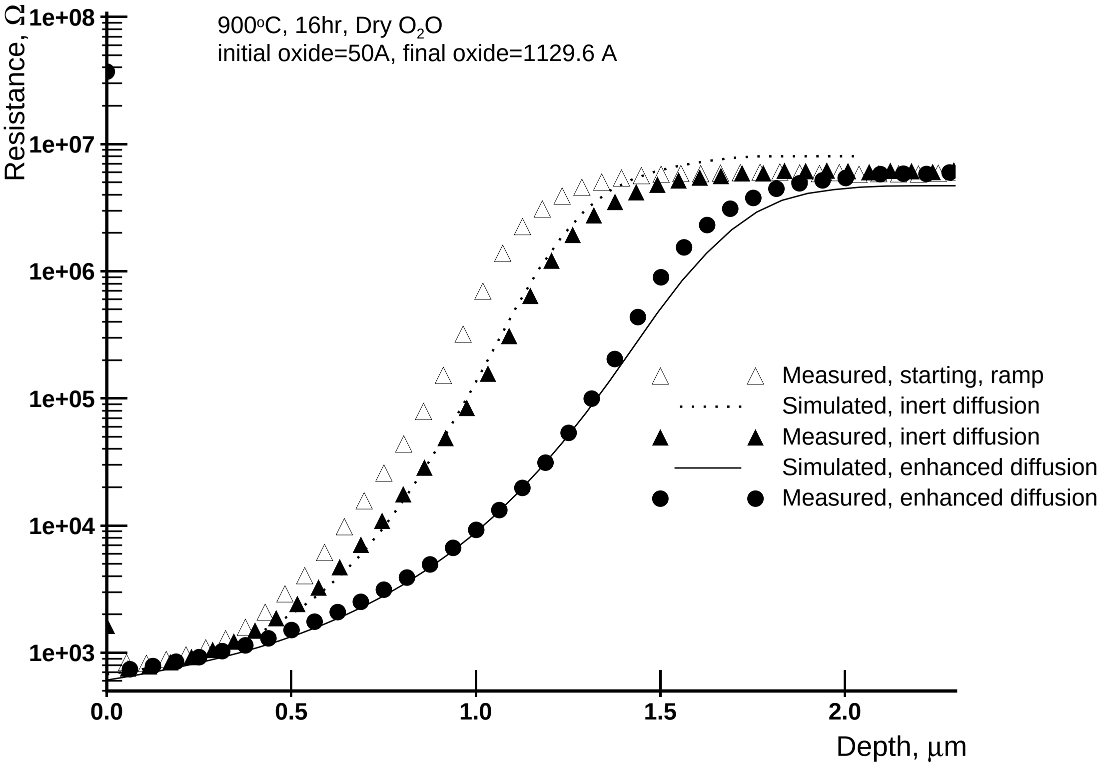

Figure 3.5: An example of the fitting calculated profile to the measured profile.

matic beam of plane polarized light is reflected off the oxide layer and also off the oxide-semiconductor interface. Since perpendicular and parallel components experience different amounts of phase shift upon reflection, by analyzing the two reflected components, oxide thickness is determined. Unfortunately the measured ellipsometric quantities are periodic functions of thickness. These thickness are known as the repeated distance of the measurement. This results in not so accurate oxide thickness measurement. For our measurements some of the oxide thicknesses (The thicker oxides) were at the repeated distance zone. To obtain a more accurate measurement we used the Nanospec and to be consistence we did all our measurements using the nanospec.

Using this data a graph of oxide thickness vs. time was plotted. Restating the Equation 2.12 we have that the oxide thickness is related to time via Deal and Grove [5] model:

$$x_o = \frac{A}{2}\left[\left(1 + \frac{t+\tau}{A^2/4B}\right)^{1/2} - 1\right], \tag{3.2}$$

Using the optimizer PROFILE the oxide thickness measured experimentally was fitted to above equation, extracting the B, B/A and τ parameters.

Chapter 4

Results and Discussions

In this chapter, we report our and discuss our experimental results. The chlorine incorporation data is addressed first. Then we look at the oxidation kinetics data. Finally, OED/ORD measurements are considered.

4.1 Incorporated Chlorine

Secondary Ion Mass Spectrometry (SIMS) was used to measure the amount of incorporated chlorine in our films. The SIMS measurements were chosen to illustrate the change in chlorine incorporation with changing time and chlorine concentrations in the gas. All of the measurements show strong incorporation of chlorine near the Si/SiO$_2$ interface. This incorporation increases for longer oxidation times (Figure 4.2 Figure 4.3), but is nearly independent of the HCl concentration (See Figure 3.2). From these results it appears that chlorine species diffuse through the oxide and react with Si at the interface. The fact that the distribution of incorporated chlorine is very nonuniform in the oxide suggests that oxidizing species react with incorporated chlorine.

It has been suggested in previous work [13] that steam generated in the gas phase can react with incorporated chlorine. To quantify the rate of this reaction, two wafers

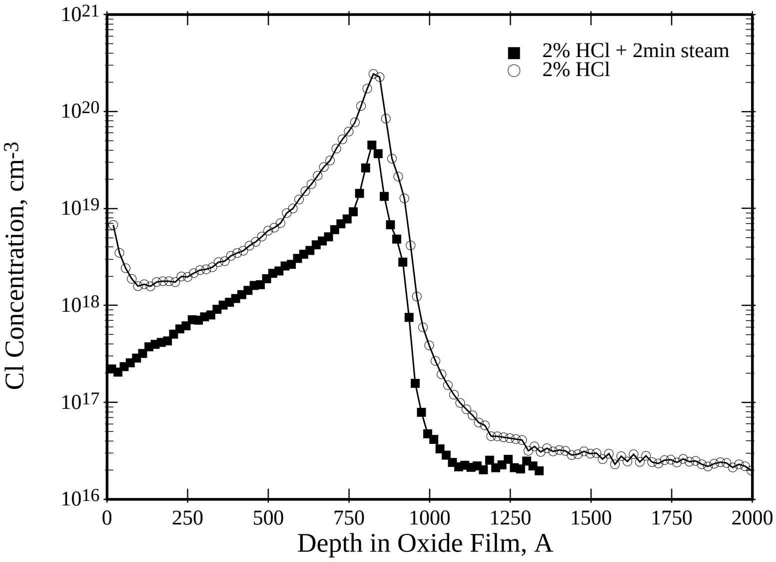

Figure 4.1: Comparison of chlorine incorporation between 2% HCl/O_2 and 2% HCl/O_2 + 2min in steam at 1000°C.

were oxidized in 2% equivalent HCl/O_2 ambient for 2h. One wafer was kept as a reference wafer and the other was oxidized in 100% steam for 2 minutes. SIMS measurements were done on both wafers and the results are shown in Figure 4.1. It can be seen that the concentration of incorporated chlorine has been reduced considerably. If we make the assumption that the concentration of steam is approximately constant across the oxide we can write:

$$\mathrm{C_{SiCl}}(t) = \mathrm{C_{SiCl}}(0)\exp(-\mathrm{t}/\tau) \tag{4.1}$$

where t is the time in the 100% steam ambient, $\mathrm{C_{SiCl}}(0)$ is the incorporated chlorine at the interface and τ is defined as:

$$\tau = \frac{1}{k\mathrm{C_{H_2O}}(0)}. \tag{4.2}$$

$\mathrm{C_{H_2O}}(0)$ is the concentration of steam at the interface and k is the reaction rate of Equation 2.21. The assumption of constant concentration of steam is a reasonable

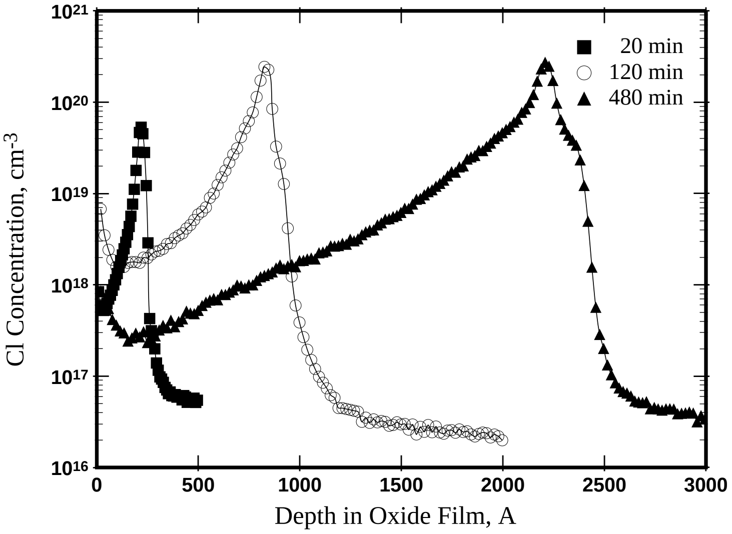

Figure 4.2: Comparison of chlorine incorporation between 20, 120 and 480min in 2% HCl/O_2 at 1000°C.

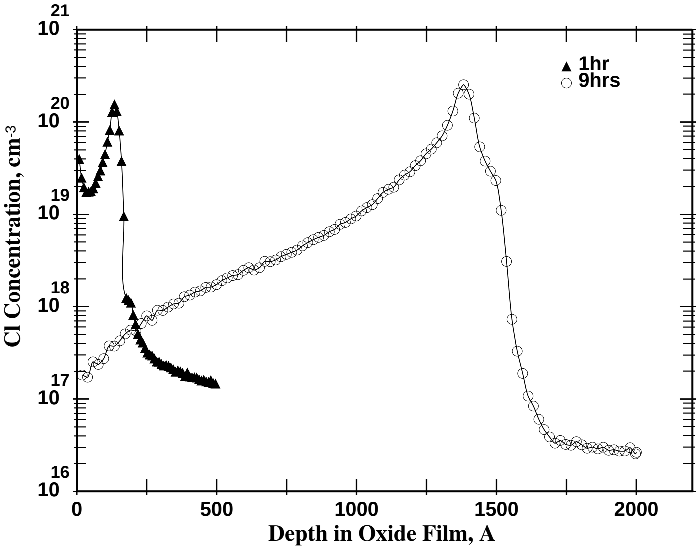

Figure 4.3: Comparison of chlorine incorporation between 60 and 540min in 2% HCl/O_2 at 900°C.

SIMS ANALYSIS

Temp	Time	HCl Press.	Q	A	L	L calculated
1000°C	20	0.02	0.1178	0.007	3.99	297.0
	160	0.02	0.5803	0.0720	7.56	219.0
	480	0.02	1.584	0.0449	20.84	140.0
	160	0.01	0.4871	0.0712	6.1974	550.0
	160	0.04	0.4783	0.0562	10.887	120.0

26 Units: Time: min., Pressure: atm, Q: nm^{-2}, A: nm^{-3}, L: nm,

Table 4.1: Conditions and results from SIMS analysis of chlorine incorporation

one, since oxidation kinetics calculation for this oxide thickness ($\approx 850\text{Å}$) shows that we are still in the linear regime where the concentration of steam species in the oxide is approximately constant. Using the above equation and the data of Figure 4.1, an average value of $k = 1.5 \times 10^{-18}$ cm^3/h was calculated. If we assume that the incorporated chlorine is immobile and the nonuniformity of the SIMS profile are mainly due to the reaction of steam via Equation 2.21,

$$\mathrm{C}_{\mathrm{SiCl}}(x) = \mathrm{C}_{\mathrm{SiCl}}(0)\exp(-\frac{x}{\mathrm{L}_{\mathrm{SiCl}}}) \tag{4.3}$$

where $\mathrm{L}_{\mathrm{SiCl}}$ is defined as:

$$\mathrm{L}_{\mathrm{SiCl}} = \frac{\frac{dx_{\mathrm{o}}}{dt}}{k\mathrm{C}_{\mathrm{H_2O}}(0)} \tag{4.4}$$

and $\frac{dx_{\mathrm{o}}}{dt}$ is the oxidation rate. To see if this model can predict the chlorine incorporation data, all the SIMS data were fitted to a Gaussian distribution convolved with an exponential plus a shifted delta function. The Gaussian was chosen to account for the broadening of the SIMS profiles, the exponential was used to extract the decay length of the incorporated chlorine near the interface, and the shifted delta function determined the location of the $\mathrm{Si/SiO_2}$ interface and accounted for the peak at the interface. An example of the fit is shown in Figure 4.4.

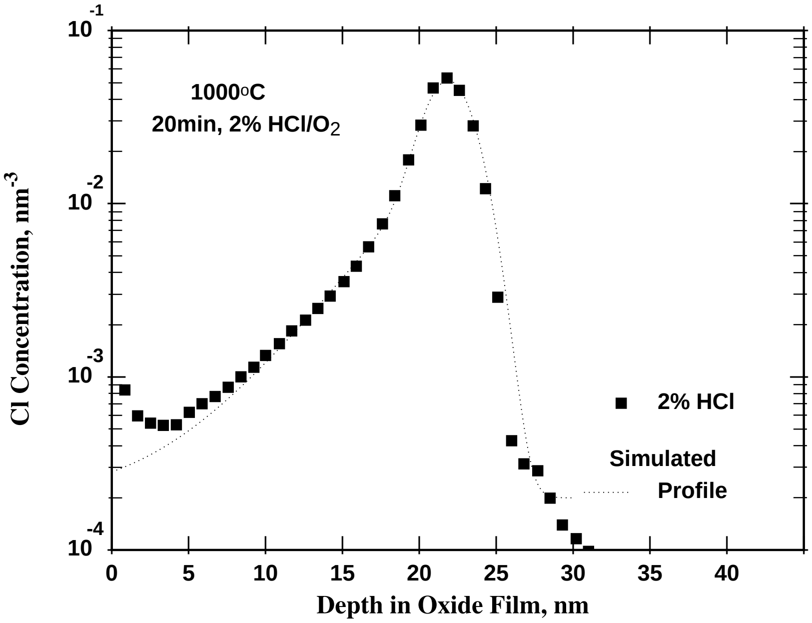

Figure 4.4: An example of a fit for chlorine incorporation, 20min oxidation 2% equivalent HCl at 1000°C.

Table 4.1 shows the dose, the preexponential factor and the decay length of the profile. In the table, the calculated decay length using the extracted reaction rate of Equation 2.21 is also included.

Comparison of the calculated decay length and experimental value of this quantity shows that the reaction of steam alone cannot account for the nonuniformity that is observed, as the decay length calculated shows a much larger value than what is experimentally observed. To explain this difference it can be noted is that the amount of incorporated chlorine at the interface increases for longer oxidation time. This increase will also effect the shape of the chlorine profiles and result in a smaller decay length as the original concentration of chlorine incorporated increases with depth into the oxide. Figure 4.5 shows the decay length and the geometric average of interface dose and the preexponential factor vs. oxidation time. It can be seen that the chlorine incorporation near the interface increases for larger oxidation time

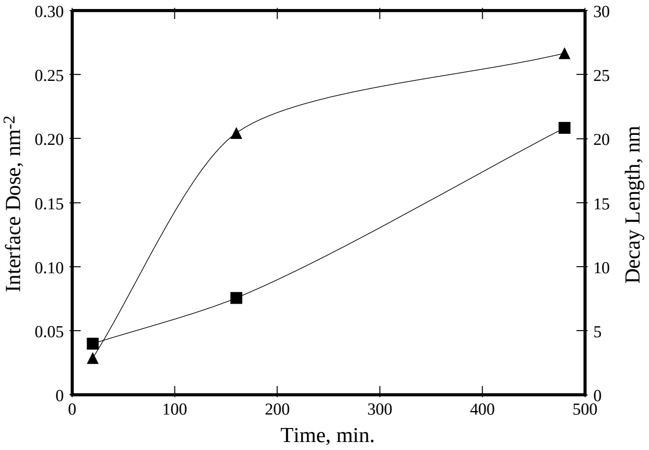

Figure 4.5: The incorporated dose factor and decay length of incorporated chlorine vs time for 2% equivalent HCl at 1000°C.

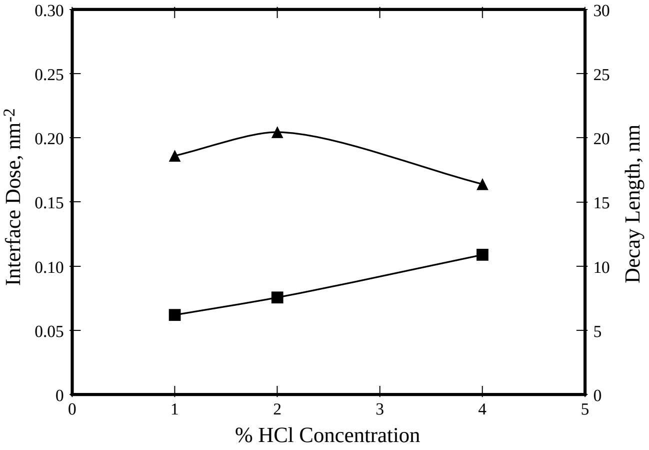

Figure 4.6: The incorporated dose factor and the decay length of incorporated chlorine vs equivalent HCl concentration at 1000°C.

and then seems to saturate. A possible explanation of the observed behavior is that at the Si/SiO_2 interface there are certain number of sites where chlorine can be incorporated. As oxidation time increases these sites fill up which results in the saturation effect seen. The decay length increases for increasing time which suggests that the chlorine incorporation with time is the dominant factor rather than to the replacement reaction involving steam which would cause L_{SiCl} to decrease as oxidation rates decreased with increasing oxide thickness.

Figure 4.6 shows the same parameters vs. partial pressure. For this figure the incorporated dose factor is approximately constant, which suggests that the interface sites are almost filled and increasing the partial pressure does not effect the incorporation anymore. The decay length again increases for larger HCl concentration. There are two processes that are in competition here. One is the chlorine incorporation at the interface and the other is the reaction of steam with the chlorinated silicon. From decay length calculations it can be concluded that the chlorine incorporation dominates.

4.2 Kinetics of Oxide Growth

As described in the Chapter 3, oxidation rates were obtained for TCA/O_2 mixtures as a function of TCA concentration and oxidation temperature. The results are shown in Figures 4.7 and 4.8, where plots of x_o vs t for various ambient concentrations at 900 and 1000°C are presented. It can be noted that the oxidation rate for all cases increase with increasing equivalent HCl concentration. Also indicated for comparison are our data for 100% dry O_2. The lines are the fit to the Deal-Grove model presented in Chapter 1, where B and B/A were calculated as was described in previous section (See Chapter 2 for more details). At both temperatures, a single value of τ was used as determined by the average of the values calculated from each equivalent HCl concentrations considered separately. All parameter fittings were done using

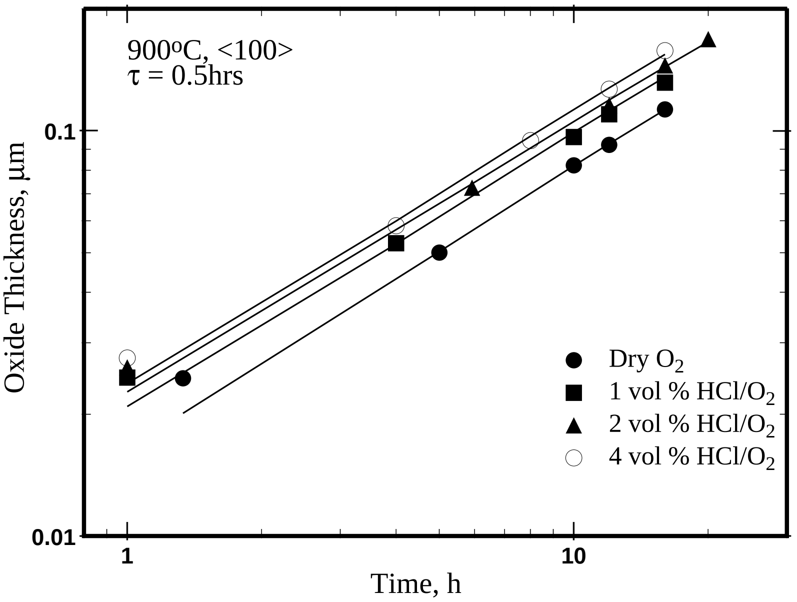

Figure 4.7: Oxide thickness vs. time for various HCl concentration at 900°C.

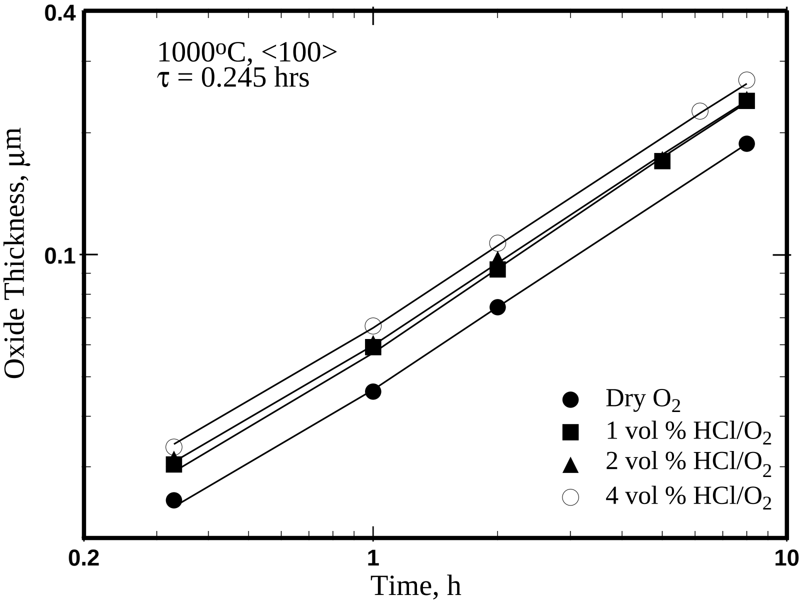

Figure 4.8: Oxide thickness vs. time for various HCl concentration at 1000°C.

PROFILE [26]. It can be seen that for the thin oxides at 900°C, the Deal and Grove model underestimates the oxide thicknesses for the shortest time. This discrepancy may be due to two factors: First, it is widely observed that thin oxides ($\leq$ 300Å) grow faster than predicted by the linear-parabolic model. Second, Nanospec supplies incident light of known wavelength and the reflected light intensity is measured as a function of wavelength. The precision of oxide thickness measurements is in the 500-10,000Å range [28]. Thus for thinner oxides, such as the ones we observe here, the accuracyy of the measurements is questionable. The thin oxides were measured using ellipsometry as well. A smaller oxide thickness was observed (about 30-50Å) when ellipsometry was used. The difference is of the right order of magnitude to account for the deviation from the Deal-Grove model.

It can be seen from the plots that the sharpest increase in the oxide thickness upon varying the HCl concentration, is the difference between dry O_2 and 1% HCl/O_2. Subsequent additions of HCl have a somewhat smaller effect, but the overall rate is systematically increased. This effect can be observed at both temperatures.

Figures 4.9 shows the result of extracting the oxidation rate constants for the Deal-Grove model. The plots are semilog plots of the effect of HCl concentration on the parabolic and linear rate constants. Also shown for comparison are the linear and parabolic rate constants calculated from steam oxidation. The concentration of steam is calculated from the gas thermodynamic calculation of Van der Mulen [16].

As can be seen from the parabolic and linear rate calculations, steam alone cannot account for the increase in the rate constants. Therefore, we conclude that chlorine species and their incorporation have an important effect on the oxidation kinetics. Inspection of these plots also show a nonlinear dependence of linear and parabolic rate constants on partial pressure of HCl, with the greatest change for small percentages. The nonlinear effect is more pronounced in the parabolic rate, which suggests that the effective diffusivity of oxidizing species is enhanced in the presence of chlorine. This effect can be attributed to chlorine incorporation, which results in greater relaxation

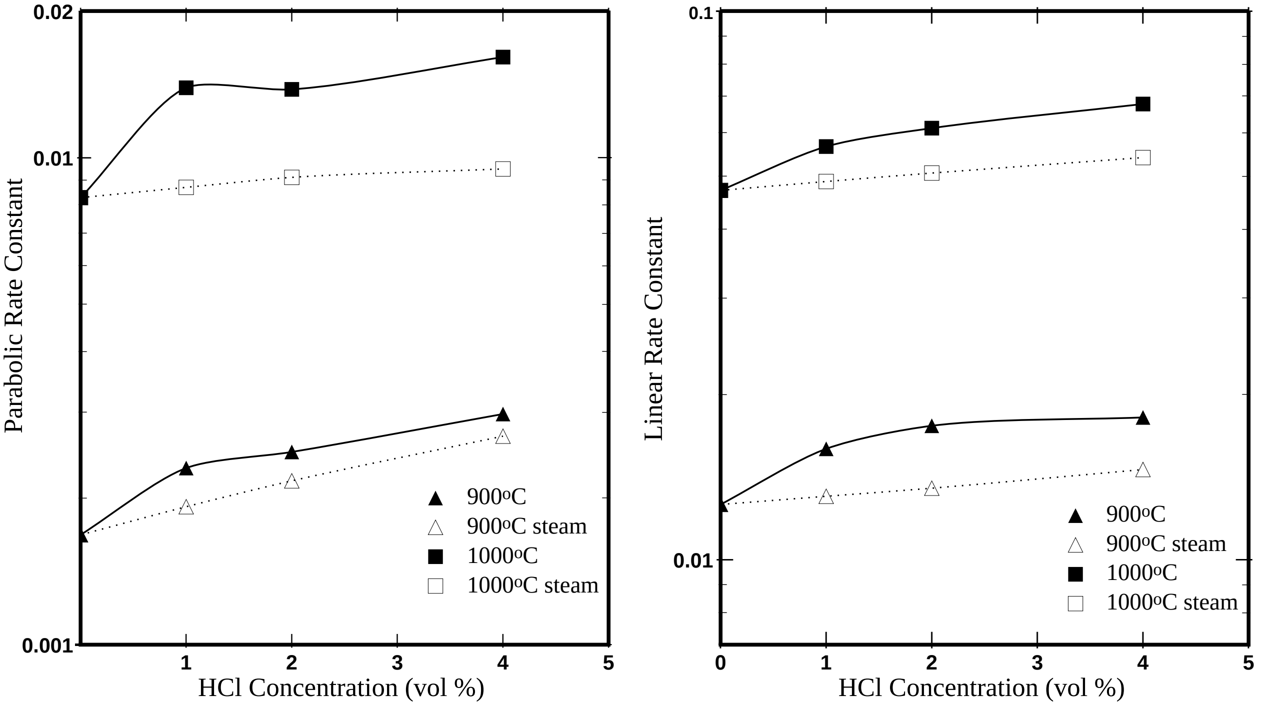

Figure 4.9: Parabolic and linear rate constants vs equivalent HCl concentration.

of the oxide. The increase in the linear rate, on the other hand, may be attributed to steam generated in the gas phase acting as a parallel oxidant. The steam react with the incorporated chlorine and provides an additional path to oxidation. This can increase the effective interface reaction rate and has a direct affect on the linear rate.

Oxide refractive index was measured as a function of equivalent HCl concentration using the ellipsometry. It was observed that the refractive index decreases for increasing HCl concentration. This further supports the assertion that the chlorine incorporation affects the structure of the oxide.

It is significant to note that the oxidation kinetics and Cl-incorporation data both show a similar trend. For addition of small amount of HCl, both data sets show a significance increase, but increasing the concentration of HCl results in a much smaller change in the linear and parabolic rate constants as well as the chlorine incorporation data. The above observation can be qualitatively explained as follows. Chlorine species in the gas phase react with O_2 to produce steam and other chlorine species. Steam and chlorine will then diffuse through the oxide to react at the interface.

Incorporated chlorine at the interface changes the structure of the oxide and allows the enhanced diffusivity of oxidizing species. On the other hand steam generated at the interface can react with the chlorinated silicon to provide an alternative path for oxidation. These reactions result in an increase in both parabolic and linear rates. Inspection of SIMS data supports the role of chlorine incorporation in the increase of oxidation rate, where small addition of HCl results both in large incorporation and enhancement of rate constants and increasing the partial pressure results in only a small change.

4.3 OED/ORD Results

Experiments were done to monitor the phosphorus diffusion profiles in presence of chlorine for 900 and 1000°C. By comparing the oxidizing and inert (nitride cap) profiles, enhanced diffusivity of phosphorus was calculated. For phosphorus, this enhancement is approximately equal to the supersaturation of interstitials (see Chapter 3 for details). The inert diffusivity calculated in this work agreed with the values reported by Antoniadis [30] for both temperatures (900 and 1000°C).

As was described previously, the diffusivity of inert and oxidizing regions was calculated by fitting the spreading resistance data using the SUPREM IV process simulator and PROFILE as an optimizer. The enhanced diffusivity is plotted as a function of HCl concentration in Figure 4.10. The by now familiar trend of the oxidation kinetics and chlorine incorporation is seen in this data as well. For addition of a small amount of HCl, there is a large reduction of supersaturation of interstitials. Increasing the HCl partial pressure results in an apparent saturation.

The role of chlorine in OED/ORD observation can be described as follows. Chlorine species in the gas diffuse through the oxide and react with the silicon at the interface. Due to incorporation of chlorine at the interface, the structure of the oxide

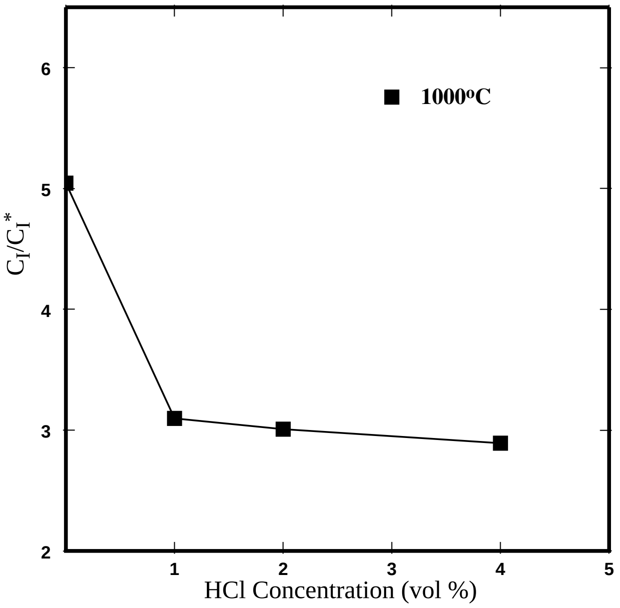

Figure 4.10: Supersaturation of interstitials vs equivalent HCl concentration at 900 and 1000°C

differs from the standard oxide. Si-Cl complex generated can act as a network terminator and result in a less rigid oxide. Thus this incorporation reduces the built-up stress in the lattice at the interface by allowing viscous flow of the oxide. Models suggests that the viscous flow [29] helps the free volume requirement at the interface, thus less Si interstitials are generated at the interface and fewer of them are available to flow into the silicon. The reaction of chlorine species at the interface can also provide another path for free volume creation. Chlorine reacts with the silicon at the interface to produce $\equiv\mathrm{Si} - \mathrm{Cl}$. The chlorinated silicon provides less stress in comparison to the case where oxygen is inserted at the interface between two silicon atoms. The Si-Cl termination also makes the network more compressible and can provide more space at the interface. All these factors can cause a reduction in the generation of interstitials and thus reduce the OED of phosphorus for increasing HCl concentration. The fact that chlorine incorporation in the film is nearly independent of the HCl concentration in the gas, leads naturally to the observed saturation effect in OED as all of the processes leading to OED reduction depend on chlorine incorporation.

Chapter 5

Conclusions and Suggestions for Future Work

In this work, we conducted a set of experiments to characterize the oxidation of silicon in chlorine containing ambients. In this section we summarize our observation and provide suggestions for further research.

The understanding of the Cl incorporation process plays a key role in the modeling of oxidation in chlorine containing ambients, since changes in the oxidation kinetics and OED/ORD behavior, depends on chlorine incorporation. We have conducted a series of SIMS measurements on the oxides grown in chlorine ambient to characterize the chlorine incorporation in the oxide. This SIMS data shows a nonuniform distribution of chlorine in the oxide. We concluded that part of this nonuniformity is due to reaction of incorporated chlorine with the water generated at the gas phase. With this assumption, we carried out an experiment to extract the rate of the reaction of steam species with the chlorinated oxide. We then tried to predict the shape of the SIMS data using our extracted reaction rate and realized that the steam replacement reaction alone cannot account for the chlorine profiles. We suggested a qualitative model in which amount of chlorine incorporated in the oxide not only depends on the reaction with steam but is also a fuction of time. SIMS data show that incorporation of chlorine increases with increasing time. This increase shows a large incorporation at shorter times and and a saturation effect for longer times. This can be attributed to the sites that are available for incorporation at the interface.

To characterize the oxidation kinetics, a series of oxide thickness measurements were done for different partial pressures of equivalent HCl at 900 and 1000°C. The oxidation rate for all cases increase with increasing equivalent HCl concentration. The largest increase in the oxide thickness, is observed between dry O_2 and 1% HCl/O_2. Subsequent additions of HCl have a somewhat smaller effect, but the overall rate is systematically increased. Parabolic and linear rate constants were extracted from the oxide thickness vs time plots. There is a nonlinear dependence of linear and parabolic rate constants on partial pressure of HCl, with the greatest change for small percentages. To account for nonlinear behavior of the parabolic rate constant we suggested that the effective diffusivity of oxidizing species is enhanced in the presence of chlorine. The increase in the linear rate, on the other hand, may be attributed steam generated in the gas phase acting as a parallel oxidant.

Finally to complete our experimental characterization of oxidation in chlorine containing ambients, we looked at the OED/ORD effects observed under influence of chlorine in the ambient. We calculated the enhanced diffusivity (or equivalently the supersaturation of interstitials) of phosphorus using spreading resistance, SUPREM IV, PROFILE and SERAPES for different partial pressures of equivalent HCl. What is observed is that for addition of a small amount of HCl, there is a large reduction of supersaturation of interstitials. Increasing the HCl partial pressure results in an apparent saturation. This observation can be explained by the incorporation of chlorine at the interface and through out the oxide. This incorporation can allow the viscous flow and provide free volume at the interface.

We can conclude from our experimental observation that chlorine incorporation in the film plays an important role in both the oxidation kinetics and the reduction of OED. It can be noted from our experiments that the dependence of parabolic and linear rate constants, reduction of supersaturation of interstitials and the chlorine incorporation on partial pressure of equivalent HCl all show a nonlinear dependence of these parameters on HCl partial pressure, with the largest change for the small addition of HCl (from 0% to 1%) and saturation effect for subsequent addition.

Continuation of this study can focus on developing a quatitative model to predict the oxidation kinetics and reduction of OED based on chlorine incorporation. Once the process of chlorine incorporation and the effect of chlorine incorporation on the processes are modeled correctly we should be able to predict the oxidation kinetics and OED/ORD behavior. The experimental results conducted in this work can be then used to extract the parameters of the model. To fully characterize the role of chlorine on OED observation, further experiments should also be conducted for different oxide thicknesses.

Bibliography

[1] R. J. Krielger, *Appl. Phys. Lett.* **20**, 449 (1972).

[2] P. H. Roginson and F. P. Heiman , *J. Electrochem. Soc.* **118**, 141 (1971).

[3] C.M. Osburn , *J. Electrochem. Soc.* **121**, 809 (1974).

[4] A. Rohatgi, S. R. Butler, and F. J. Feigl *Appl. Phys. Lett.* **30**, 104 (1977).

[5] B. E. Deal and A. S. Grove, *J. Appl. Phys.* **36**, 770 (1965).

[6] M. B. Das, J. Stach and R. E. Tressler, *J. Electrochem. Soc.* **131**, 389 (1984).

[7] E. J. Janssens and G. J. Declerck, *J. Electrochem. Soc.* **125**, 1697 (1978).

[8] J. R. Flemish and R. E. Tressler, *J. Electrochem. Soc.* **135**, 1192 (1988).

[9] B. E. Deal, D. W. Hess, J. D. Plummer and C. P. Ho, *J. Electrochem. Soc.* **125**, 339 (1978).

[10] Bruce E. Deal, *J. Electrochem. Soc.* **125**, 576 (1978).

[11] K. Hirbayashi and J. Iwamura, *J. Electrochem. Soc.* **120**, 1595 (1973).

[12] A. Rohatgi, S. R. Butler, and F. J. Feigl *J. Electrochem. Soc.* **126**, 143 (1979).

[13] Y. D. Sheu and S. R. Butler and F. J. Feigl , *J. Electrochem. Soc.* **133**, 2136 (1986).

[14] Zhi Ling, Luc Dupas and Kristen M. De Meyer , *private communication.*

[15] J. R. Monkowski, Michael D. Monkowski, I. S. T. Tong and J. Stach, Silicon processing, ASTM STP 804 American society for testing and Materials, 245 (1983).

[16] Y. J. van der Meulen and J. G. Cahill, Journal of Electronic Materials **3**, 371 (1974).

[17] C. P. Ho and J. D. Plummer, *J. Electrochem. Soc.* **126**, 1516 (1979).

[18] S. T. Dunham and D. J. Plummer, *J. Appl. Phys.* **59**, 2541 (1986).

[19] Yasumasa Nabeta, Tadashi Uno and Hirokazu Tsukamoto , *J. Electrochem. Soc.* **123**, 1416 (1976).

[20] Ravi Subrahmanyan, Hisham Z. Massoud and Richard B. Fair, *Appl. Phys. Lett.* **61**, 4804 (1987).

[21] Takeshi Hattorir, *J. Electrochem. Soc.* **123**, 945 (1976).

[22] Hiromitsu Shiraki, *J. Appl. Phys.* **15**, 1 (1976).

[23] Seajin Oh and W. A. Tiller, *Appl. Phys. Lett.* **48**, 1125(1986).

[24] Ed tierney , *TCA Process Calculation for Process Engineers* J. C. Shumacher.

[25] M. E. Law, C. Rafferty, and R. W. Dutton, "SUPREM IV Users Manual" Technical Report, Integrated Circuits Lab., Stanford Univ., Jul. 1986.

[26] Gertjan L. Ouwerling, "Profile/Prof2d User's Manual" Delft University of Technology, Electrical Materials Lab., Jul. 1989.

[27] P. M. Fahey, P. B. Griffin, and J. D. Plummer, Rev. Modern Phys. **61**, 289 (1989).

[28] Ghandi, VLSI Fabrication Principles

[29] T. Y. Tan, U Gösele, and F. F. Morehead, *Appl. Phys. Let.* **39**, 86 (1981).

[30] A. Lin, D. A. Antoniadis, and R. W. Dutton, *J. Electrochem. Soc.* **128**, 1131 (1981).

[31] B. E. Deal, A. Hurrle and M. J. Schultz, *J. Electrochem. Soc.* **125**, 2024 (1978).